8-2009

Single Molecule Detection of Near-Infrared Phthalocyanine Dyes

You Li

University of Tennessee - Knoxville

To the Graduate Council:

I am submitting herewith a thesis written by You Li entitled "Single Molecule Detection of Near-Infrared Phthalocyanine Dyes." I have examined the final electronic copy of this thesis for form and content and recommend that it be accepted in partial fulfillment of the requirements for the degree of Master of Science, with a major in Physics.

Lloyd M. Davis, Major Professor

We have read this thesis and recommend its acceptance:

Horace W. Crater, Christian G. Parigger

Accepted for the Council:
Carolyn R. Hodges

Vice Provost and Dean of the Graduate School

(Original signatures are on file with official student records.)

To the Graduate Council:

I am submitting herewith a thesis written by You Li entitled “Single Molecule Detection of Near-Infrared Phthalocyanine Dyes.” I have examined the final electronic copy of this thesis for form and content and recommend that it be accepted in partial fulfillment of the requirements for the degree of Master of Science, with a major in Physics.

Lloyd M. Davis, Major Professor

We have read this thesis
and recommend its acceptance:

Horace W. Crater

_____

Christian G. Parigger

_____

Accepted for the Council:

Carolyn R. Hodges

_____

Vice Provost and Dean of the Graduate School

(Original signatures are on file with official student records)

Single-molecule detection of near-infrared phthalocyanine dyes

A Thesis Presented for

The Master of Science

Degree

The University of Tennessee, Knoxville

You Li

August 2009

Dedication

This thesis is dedicated to my dear parents: my beloved father Jianfu Li and my beautiful mother Fuling Wang.

Acknowledgements

This research has been supported by grant R01 EB-006639 from the National Institutes of Health. I would like to express my gratitude to my advisor, Lloyd Davis. The writing of this thesis could not have been completed without his patience and guidance. I am also deeply indebted to Dr Brian Canfield, who helped me throughout my research and in the writing of this thesis. Also, many thanks go to my committee members: Dr Christian Parigger and Dr Horace Crater for their support and suggestions on this thesis. I would also like to thank the friends I've made at UTSI. I had a really good time here with you guys.

Abstract

The major advantage associated with near-infrared monitoring is the fact that few compounds show intrinsic fluorescence in this region of the spectrum and hence background from other molecules is reduced. Phthalocyanine dyes provide emission at deep red and near infrared wavelengths but have excellent photostability and hence are an attractive candidate for near-infrared fluorescence bioassay applications. However, because of their small Stokes shifts, non-standard methods are needed for optimum separation of fluorescence from scattered laser light. This thesis reports the development of a custom confocal microscope that uses a low-cost laser diode operating at 667 nm for sample excitation and an angle-tuned Raman notch filter to block scattered laser radiation and provide high-throughput of fluorescence with small Stokes shift. Also, a diffraction grating is used to isolate the laser excitation wavelength from the broadband luminescence of the laser. The experimental system is used to observe photon bursts from single molecules of zinc phthalocyanine fluorophores in an ethanol solution. The autocorrelation function of the photon trace, which is measured in fluorescence correlation spectroscopy, provides a measure of the presence of photon bursts from single molecules. Experiments to characterize the limits of detection of near-infrared fluorophores in aqueous solution using the microscope are also discussed.

Table of Contents

List of Tables

List of Figures

Chapter I

Introduction

Modern pharmaceutical drug discovery makes use of high-throughput screening (HTS) technology in which large libraries of chemical compounds (containing 100,000 or more different types of small molecules) are screened to find those that interact with or modify the biological function of a target protein or enzyme, which has been identified from prior molecular-biology knowledge [1] .

A major cost of HTS is for the chemicals and biological molecules. Therefore there is a need to minimize the quantities of samples needed for the physical assays of the molecular interactions. Fluorescence spectroscopy provides one of the most sensitive means for detecting molecules and has achieved sensitivity at the single-molecule level for many years [2]. Fluorescence has the potential for making measurements with very small volumes of samples. The goal of the research in this thesis is to develop a low-cost instrument for sensitive fluorescence detection in the deep red or near-infrared (near-ir) regions of the spectrum. Such an instrument could be used to make measurements for HTS applications using low-cost microfluidic devices made from poly-methyl methacrylate (PMMA), which is a plastic material that can be molded to form so-called lab-on-a-chip devices at very low cost [3]. Unfortunately, PMMA exhibits its own fluorescence (this is called autofluorescence), and this can cause a significant background in measurements of other fluorescent targets. Also, many of the chemicals to be tested in HTS exhibit autofluorescence.

Therefore, in this research an instrument for deep-red or near-ir fluorescence detection is of interest, because few compounds show autofluorescence in this of the spectrum and thus background from the PMMA and other molecules will be reduced. Hence, the objective of this research is to design and construct a simple

compact time-resolved fluorescence microscope for reading fluorescence and detecting single molecules of a near-ir dye in solution. The instrument makes use of processing of the fluorescence signal by the technique of fluorescence correlation spectroscopy (FCS). This technique was first established in the early 1970's as an extension of photon correlation spectroscopy methods for determination of particle diffusion kinetics by dynamic light scattering [5]49. In HTS, FCS may be used for measuring if a small fluorescently labeled molecule interacts with a large target protein, because the rate of diffusion of the fluorescent molecule is much slower it binds to the protein [6].

FCS is a versatile method for characterizing the dynamics of a low number of fluorescent molecules moving through a very small detection volume, normally the laser focus in a confocal microscope [7]**.** It is used in numerous biophysical studies and has many applications in analytical chemistry and biochemistry. A range of molecular dynamic processes that affect the fluorescence intensity may be by FCS. The widespread use of FCS as a routine tool for bioscience investigations has become possible due to improvements in signal-to-noise of detectors, with technical developments such as the demonstration of single-molecule detection in solution, the use of confocal microscopy with a high numerical aperture (NA) objective to reduce the sample volume, and the application of high quantum-quantum-efficiency single-photon avalanche-diode (SPAD) detectors [8].

Chapter II begins with a brief section on fluorescence fundamentals. Properties of phthalocyanine dyes are discussed in Section 2.2, including the small Stokes shift, which is relevant to the design of the instrument. Section 2.3 makes clear the advantages and basis of confocal microscopy, which factor into the instrument configuration and alignment; Section 2.4 explains the function of the Raman notch filter; Section 2.5 gives information on the single photon avalanche diode (SPAD) detector used in the instrument; and Section 2.6 elucidates the use of the technique of FCS. Chapter III focuses on the instrument built for this thesis, beginning with the

optical layout, alignment procedure, and optimization of the confocal condition. Details of key optical components are presented. Data collection and processing procedures are explained, including the correction for detector afterpulses from the SPAD. Chapter IV presents sample preparation procedures and the results of measurements to detect minute quantities of zinc phthalocyanine dye in solution by use of fluorescence photon counting and by FCS. Chapter V is a summary of the thesis and suggestions for future work.

Chapter II

Background Information

2.1 Fluorescence fundamentals

Fluorescence occurs when a photon of light is absorbed by a molecule (known as "fluorescent label") thereby raising it to an exited state. Figure 1 shows the energy levels of a fluorescent molecule, including the sublevels in the ground state (S_0), the excited state (S_1), and the triplet state (T_1). When a molecule absorbs a photon of light and is excited, it goes to a particular sublevel of the S_1 manifold and then very rapidly to the lowest sublevel of S_1. It may cross to the T_1 manifold and then decay by phosphorescence, as shown by the dashed arrows in the figure. However, most of the time, it will emit a fluorescence photon as it decays directly to an excited sublevel in S_0. The energy difference between the excitation and the fluorescence emission (yellow and red lines in Figure 1) is called the Stokes shift [9]. This is an important quantity for the near-ir dyes used in this work.

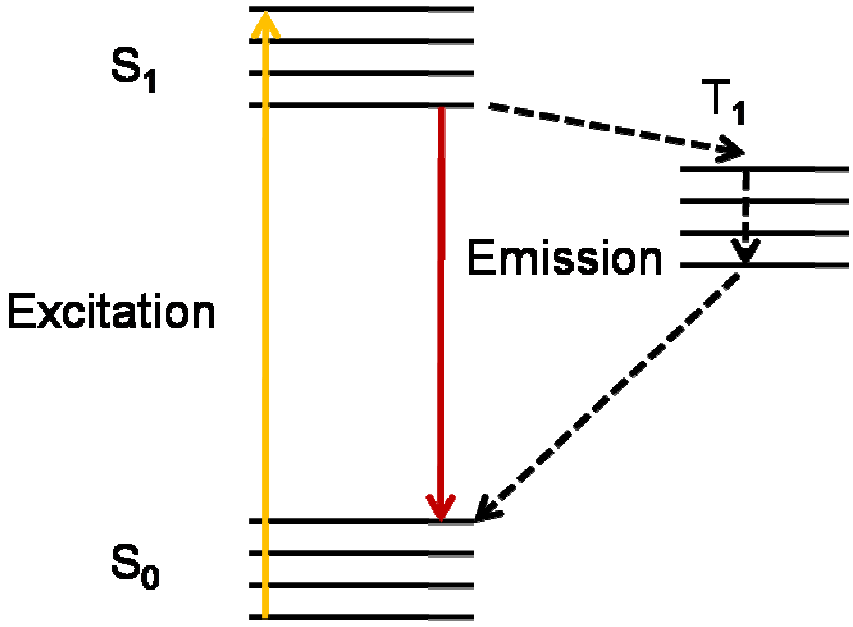

Figure 1 The Jablonski diagram of a fluorescent molecule

2.2 Phthalocyanine dyes

The focus of this thesis involves sensitive fluorescence detection in the deep red or near-ir regions of the spectrum. Most near-ir fluorophores exhibit poor chemical stability especially in aqueous solution and also readily photobleach on exposure to light [8][8]. However, phthalocyanine dyes provide excellent photostability and chemical stability and hence are an attractive candidate for fluorescence bioassay applications [10].

Phthalocyanines are particularly of interest due to their high extinction coefficients; typically it's about $\varepsilon=2.85\times10^5$ M^{-1} cm^{-1}. By comparison, for the commercially available Alexa 660 dye, $\varepsilon= 1.32\times10^5$ M^{-1} cm^{-1}. They also have favorable fluorescence quantum yields in the range of 0.40–0.41 with different degrees of carboxylation; for example, for the zinc phthalocyanine (ZnPc) used in this thesis, the quantum yield is 0.41 [11] The chemical structure indicates that ZnPc is chemically robust and photochemically stable due in part to the nitrogen atoms located within aromatic macrocycle and the peripherally fused benzene rings, as seen in Figure 2.

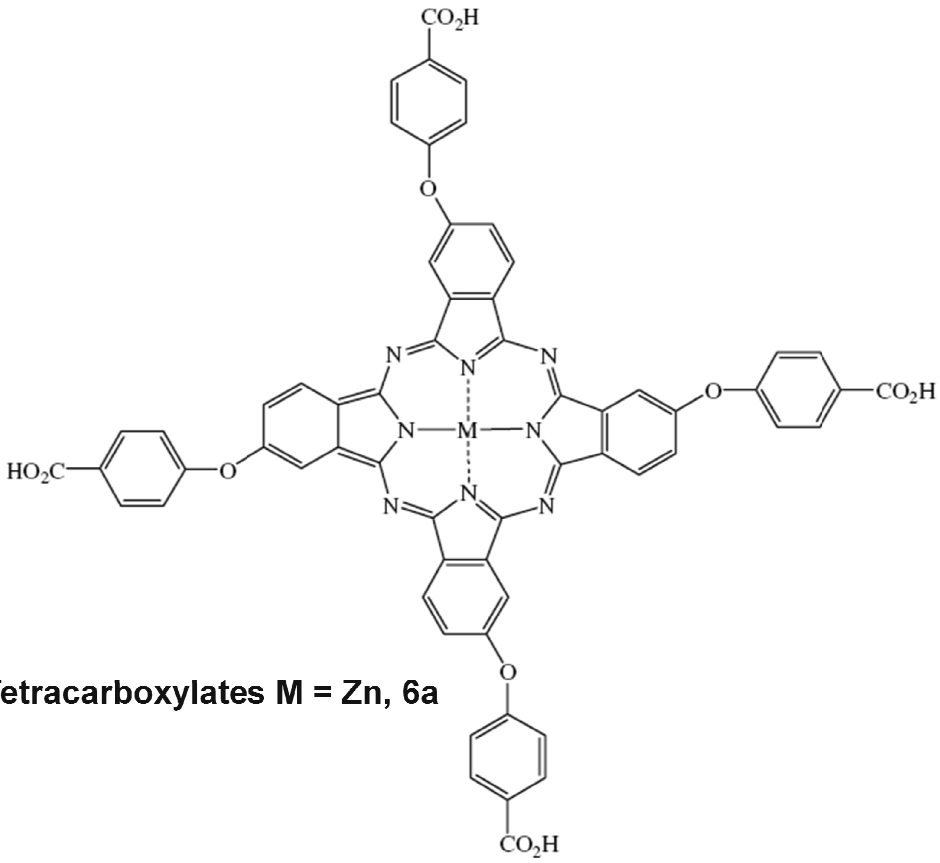

Figure 2 Chemical structure of ZnPc dye (from Ref. [11])

These dyes possess a strong absorption band in the near-ir due to the extended π-conjugation system around the ring structure. In the case of ZnPc, the 667 nm laser diode wavelength can be used for excitation, as seen in Figure 3. (The absorption and emission spectra for this graph were provided by Dr. Irina Nesterova and Dr. Steven Soper, from Louisiana State University.) However, ZnPc has a very small Stokes shift, which means that the difference between the absorption wavelength peak at 677 nm and the emission wavelength peak at 687nm is only as small as 10 nm. Note that the small peak in the absorption spectrum at ~615 nm is thought to be due to non-fluorescent aggregates.

Because of the small Stokes shift, non-standard methods are needed for optimum separation of fluorescence from scattered laser excitation light. Section 2.4 the use of an angle-tuned Raman notch filter for this purpose, which results in the

transmission curve shown by the dark blue line in Figure 3. Also in Figure 3, the red line indicates the 666.92 nm wavelength where the diode laser excites the dye molecule, which will also be filtered out by the Raman notch filter. Although a small portion of the ZnPc dye emission light will be cut off by the filter, the major part of the fluorescence still can get through the Raman notch filter. However, as discussed at the end of section 2.4, experimental results were collected with an additional bandpass filter used before the detector. The transmission of this filter is shown in Figure 3 as the light blue line. This filter reduces background by blocking Raman scattered light from solvent molecules, which occurs at wavelengths ~730—870 nm, but it also reduces the fluorescence signal. The yellow line in Figure 3 shows the transmission of another bandpass filter, which also blocks the Raman scatter from solvent molecules, but which passes the peak of the ZnPc fluorescence spectrum. This filter is being used in continuing research.

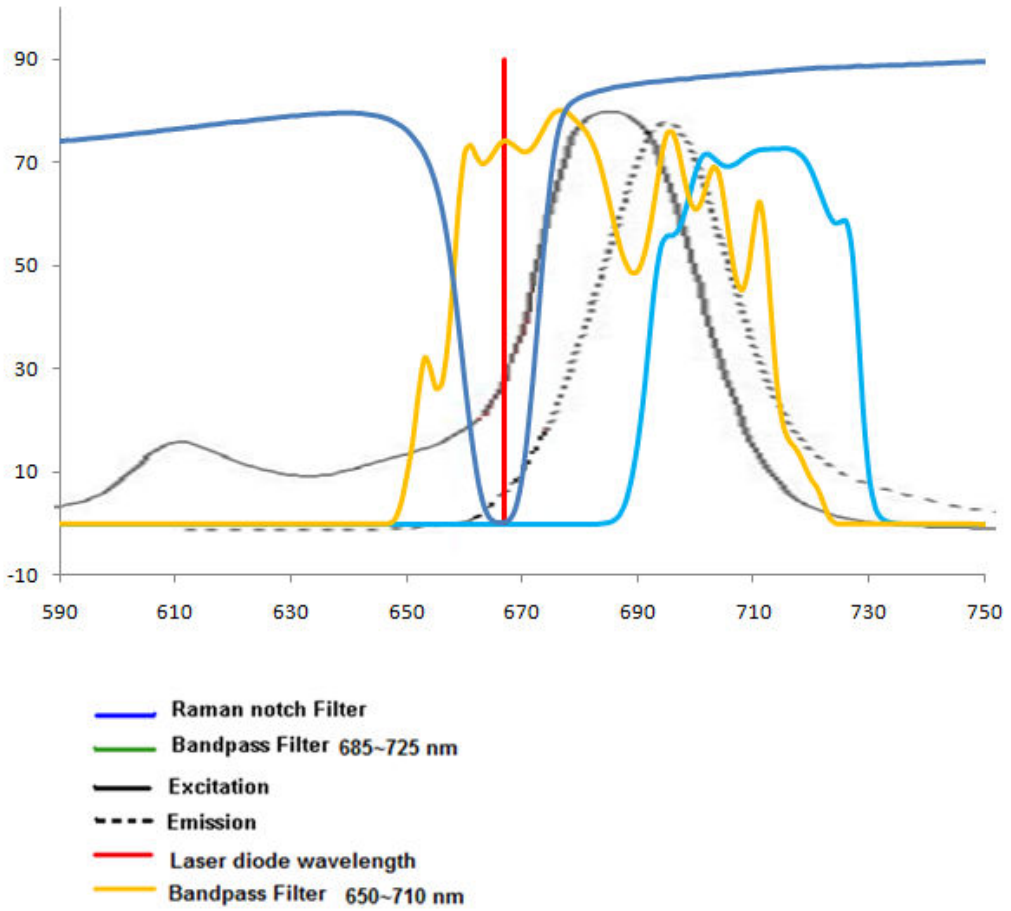

Figure 3 Normalized absorption and emission spectra of ZnPc dye and transmission spectra of the Raman notch and bandpass filters

2.3 Confocal microscopy

In this thesis, a custom made confocal microscope is developed for detection of the ZnPc dye. The confocal technique is widely used in fluorescence experiments in a variety of research areas such as biology and medicine. A main advantage of confocal microscopy is its ability to scan the surface and to produce three dimensional images of thick objects. This is possible because it allows optical sections to be imaged with minimal blur from other parts of the sample. In conventional fluorescence microscopy the object is uniformly illuminated and each point of the object is imaged by the objective lens. Thus the objective is responsible for determining the contrast and resolution of the system. The confocal microscope achieves superior contrast by placing an exit pinhole conjugate to the spot being scanned so that only the light originating from the scanned spot is transmitted through the pinhole.

Figure 4 shows an expanding beam from an excitation laser source, which is directed by a dichroic mirror into a high-NA microscope objective, which focuses the light inside the sample at the focal plane. The fluorescence emission from the sample is collected through the same high power objective and focused onto a pinhole, so that the part of the sample that is illuminated by the laser beam waist is imaged onto the pinhole aperture. Out-of-focus information is rejected by the pinhole, so that only the confocal plane is imaged. After the pinhole, the fluorescence signal can be collected by a photon counting detection system. In this work, a single-photon avalanche diode (SPAD) detector (Perkin Elmer SPCM-14) is used and is discussed in Section 2.5.

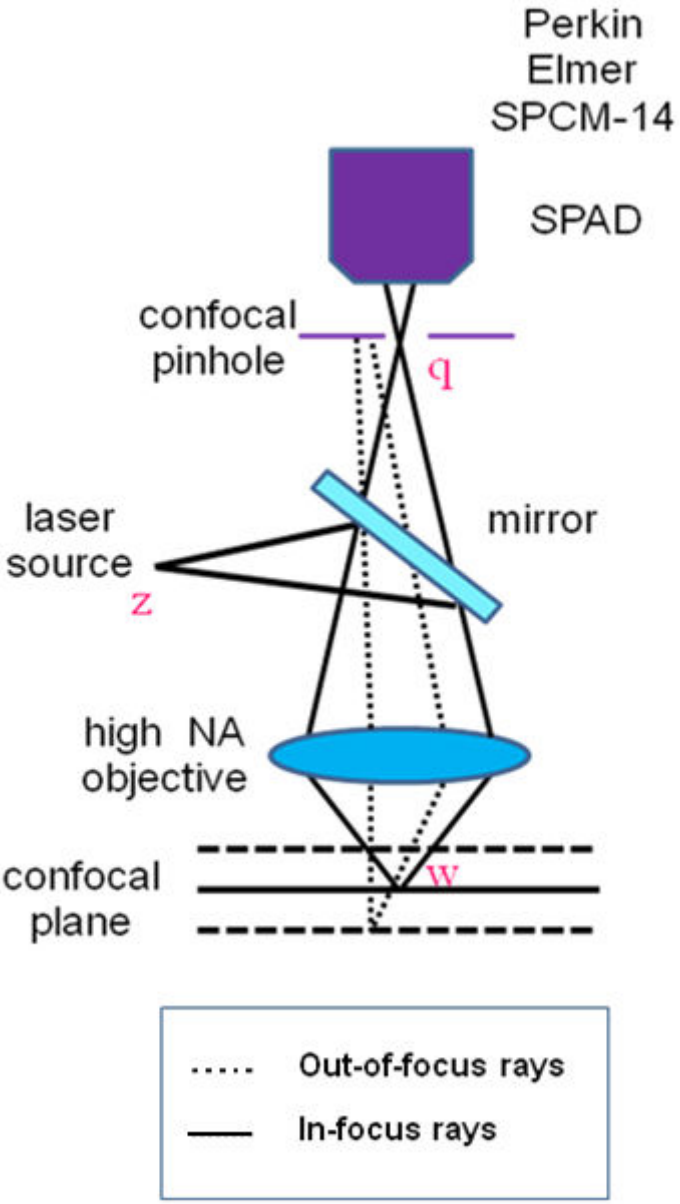

Figure 4 Confocal microscope configuration

In Figure 4, the two points z and w are known as "conjugate points". The focal point of the objective lens of the microscope (w) forms an image at the location of the pinhole (**q**). Hence, the pinhole is conjugate to the focal point of the lens, thus it is a confocal pinhole. Now the three points (**q**, **w** and **z**) are all mutually confocal—hence the name.

A photo of the confocal microscopy setup during construction is shown in Figure 5.

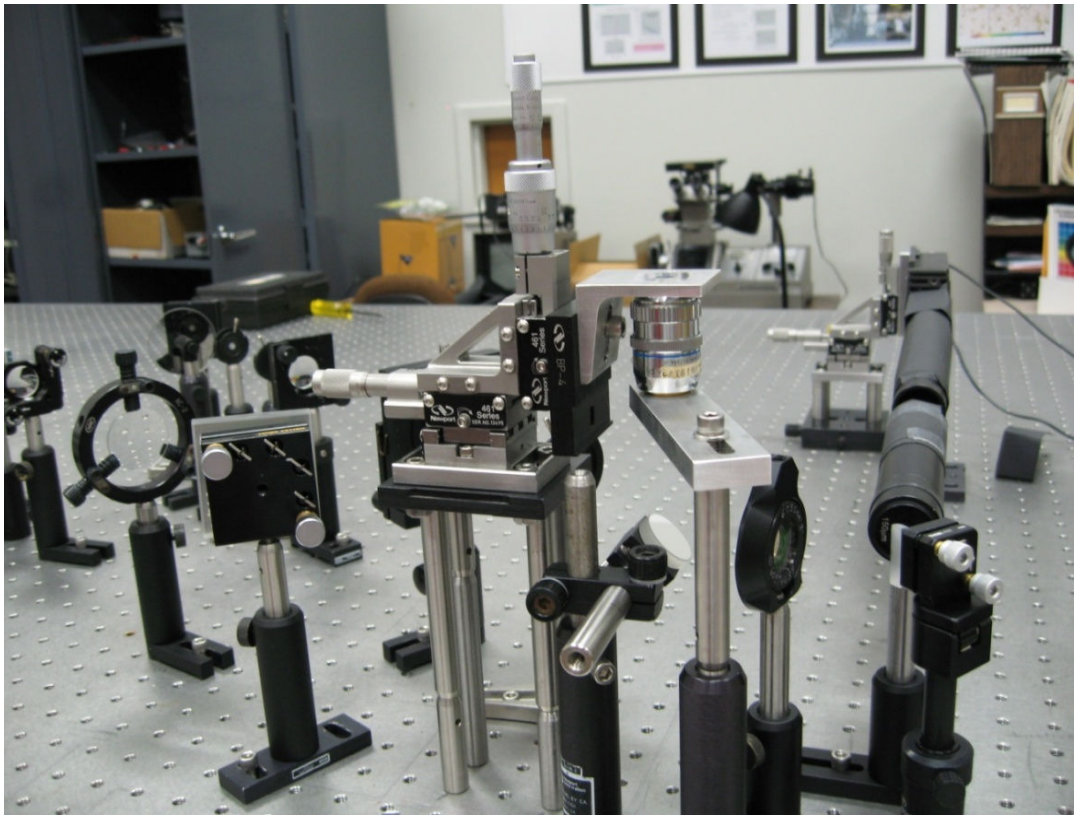

Figure 5 Photo of experimental setup during construction

Due to the Stokes's shift, the wavelength of fluorescence emission is longer than the excitation wavelength. It is this shift in wavelength that makes it possible to observe the emitted light. The typical confocal microscope setup uses a conventional dichroic mirror, which reflects the excitation light towards the objective and to the sample, as seen in Figure 6. However, light emitted by the fluorescent molecules is collected by the objective and passes through the dichroic filter towards the detector. Most of the scattered excitation light is reflected from the dichroic filter back towards the laser. As seen in Figure 6, an appropriate emission filter may also be used to stop any small portion of the scattered excitation light that may pass through the dichroic mirror.

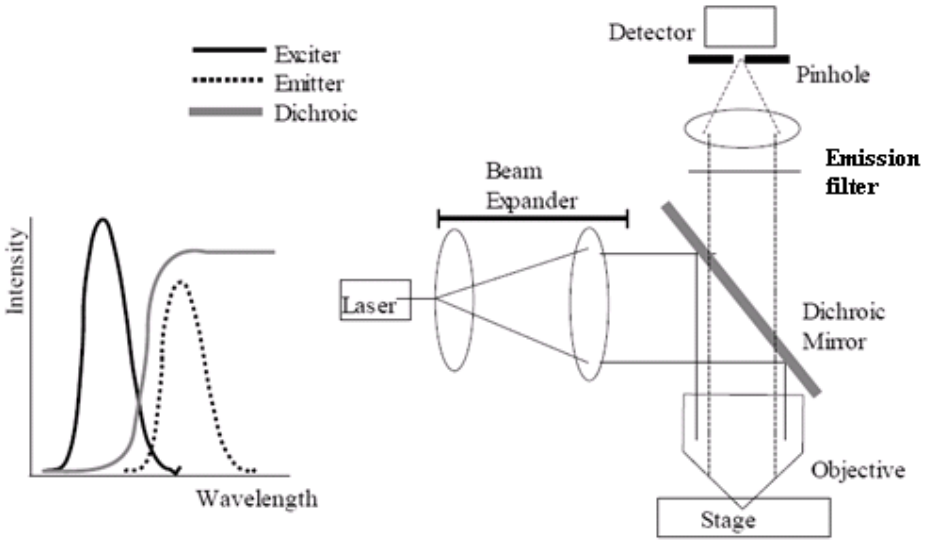

Figure 6 Typical confocal microscope using a dichroic mirror

However, the ZnPc dye has a very small Stokes shift as stated in Section 2.2, and hence a non-standard method is needed to improve the signal-to-noise ratio. The key properties of the Raman notch filter and how it works to achieve this objective in the setup are discussed in detail in the following section.

2.4 Use of a Raman notch filter

A Raman notch filter is so named because it is often used in Raman spectroscopy to block Rayleigh scattered laser light (i.e., elastically scattered light) while transmitting Raman lines, which are at slightly longer wavelengths but very close in wavelength to the laser wavelength. Unlike an interference filter, which consists of discrete layers of different refractive indices, the Raman notch filter is made by a holographic process and consists of a sinusoidally varying refractive index profile. The SuperNotch-Plus™ filter from Kaiser Optical (www.kosi.com) provides blocking of the laser wavelength with optical density (OD) of > 6.0 and a spectral bandwidth between the 50% transmission points of < 350 cm^{-1}, which corresponds to about 10 nm for a center wavelength of 672 nm. More importantly, the spectral edgewidth, which is defined as the wavenumbers between the points on the transmission curve with OD of 0.3 and 4.0, is < 150 cm^{-1}. Solving $1/\lambda_1 - 1/\lambda_2 = 150\ cm^{-1}$, with λ_1 = 667 nm with (the diode laser wavelength) gives λ_2 = 673.7 nm, and thus the spectral edgewidth is only 6.7 nm.

The experiments reported in this thesis use a Raman notch filter (Holographic SuperNotch® Plus from Kaiser Optical system, Inc) that is custom made for a center wavelength of 673 nm. The filter is angle tuned at an appropriate angle to reflect the excitation laser, as seen in Figure 7. At the same time, one must also take into account if the fluorescence light from the ZnPc dye can get through the filter efficiently.

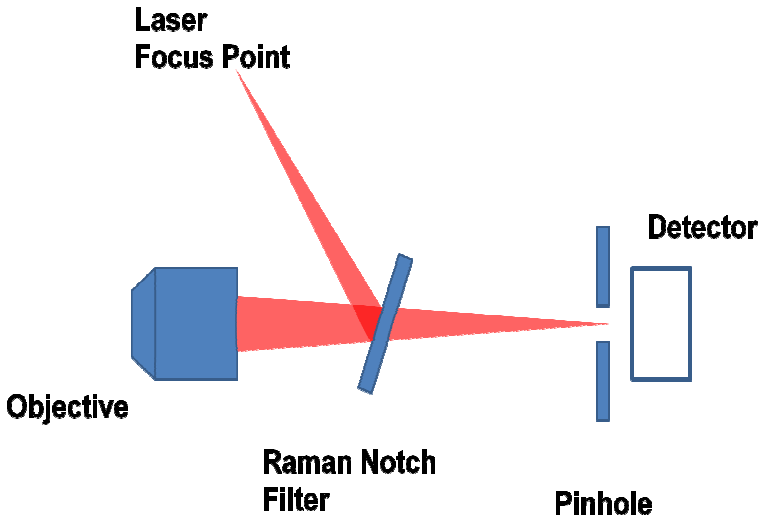

Figure 7 Use of Raman notch filter for confocal setup

Note if a bandpass interference filter is used to further attenuate scattered excitation light that may pass through the Raman notch filter and pinhole, as is done in the conventional setup of Figure 6, then there is a potential for further loss of fluorescence because the spectral edgewidth of a bandpass interference filter is not as sharp as that of the Raman notch filter. An additional filter is used in the experimental setup for filtering out the Raman scatter from the solvent. In the results reported in Chapter IV, a filter is used which has a bandpass from 685 nm to 725 nm (shown as the light blue line in Figure 3). Raman scattered light from the solvent molecules is due mostly to the O-H stretch (~3000 cm^{-1}) and O-H bend mode cm^{-1}), which for 667 nm excitation, falls at wavelengths from ~730—870 nm. After insertion of the bandpass filter, the background is reduced from 2000 s^{-1} down to $s^{-1,}$ which is close to the 110 s^{-1} measured dark count rate of the SPAD. However, bandpass filter cuts off a significant portion of the fluorescence from the ZnPc dye. Hence in continuing research a filter with a bandpass from 650 nm to 710 nm (shown as the yellow line in Figure 3) is being used.

2.5 Single photon avalanche diode (SPAD)

The detector used in this work is a single-photon counting module (Perkin Elmer SPCM-14) containing a single-photon avalanche diode (SPAD) operated with an active quenching circuit [12]. At the fluorescence wavelength of 680-720 nm, the single-photon detection efficiency is about 65-70%. The detector is specified to have a dark count rate of < 150 s^{-1}, and the afterpulse rate (discussed in Section 3.7.1) is 0.1%. The active area of the detector has a diameter of only ~ 150 microns, and hence tight focusing of the light to be detected and careful alignment are needed, as discussed in Section 3.2.

The SPAD is essentially a p-n junction reverse biased above the breakdown voltage such that the junction electric field is sufficiently high to sustain the flow of an avalanche current triggered by a photogenerated carrier [13]**.** Thus the SPAD is like a bistable triggering circuit with a very large gain (>10^5), sufficient for the detection of single photons. By contrast, an ordinary avalanche photodiode (APD) is operated below the breakdown voltage as an analog amplifier with modest gain (~250) and large dynamic ranges for use in applications with medium-to-high light levels. To reduce thermally generated dark counts and ensure fast single-photon timing, are designed with considerably smaller active areas than APDs.

Ultrasensitive detection and spectroscopy experiments require detectors with single-single-photon detection capability, high quantum efficiency, and low dark noise. Also, for time resolved spectroscopy and time-gated detection schemes a detector with subnanosecond single-photon timing jitter is needed. The first experiments for the detection of single dye molecules in solution used a microchannel plate photomultiplier to achieve most of these requirements except that the quantum efficiency was only 5—8%. Therefore considering the higher quantum efficiency, together with adequate time response and dark count rate, the experiments in this

thesis use a single-photon avalanche diode (SPAD). The SPAD detector is also now the detector of choice in experiments for fluorescence correlation spectroscopy (FCS).

2.6 FCS fundamentals

The approach taken for the single-molecule detection of the Alexa 660 and zinc-zinc-phthalocyanine (ZnPc) near-ir dyes used in this thesis is based on fluorescence correlation spectroscopy (FCS), in which the motion of a fluorescent species is monitored by collecting the autocorrelation function (ACF) of the stream of detected photons to analyze fluctuations in fluorescence emission coming from a tightly focused laser spot. Due to the power of statistical averaging, the FCS technique allows to measure the presence of fluorescence concentrations well below 100 picomolar [14].

The probe volume in a FCS setup is defined by a light beam, which traverses the sample [15]. As the molecules appear in or disappear from the light beam, either due to diffusion or chemical reaction, their concentration fluctuations give rise to corresponding fluctuations of the intensity of emitted fluorescence. Observation of these spontaneous fluctuations can yield a kinetic description of the system equivalent to that obtained by conventional means. FCS takes advantage of the fluorescence changes that can result from chemical reactions and so increases the feasibility of observing the decay of concentration fluctuations via these reactions. Another advantage of fluorescence detection is its chemical specificity, which proves useful in interpreting complex kinetic measurements and in observing particular reactions in complex mixtures such as biological systems.

Chapter III

Experimental setup and data analysis

This chapter provides a detailed description of the confocal microscopy setup used for single-molecule detection. Also details of the alignment procedure, optical components, and the data collection and analysis are presented.

3.1 Optical layout

The optical layout of the confocal microscope developed in this research is sketched in Figure 8 and the corresponding photo is provided in Figure 9.

The sample excitation is provided by the beam from a continuous-wave diode laser (Thorlabs CPS67HP05-SE), operating at 667 nm. This is specified to have 5 mW of light output. The diode laser output beam is elliptical and so the beam is first passed through a round iris. In order to facilitate the optical alignment of the experiment, the beam from a Helium Neon (HeNe) laser is combined with the diode laser beam at a non-polarizing prism beamsplitter.

In initial experiments, the diode laser beam was found to have broadband luminescence collinear with the 667 nm beam. To filter this luminescence, a holographic diffraction grating (1200 lines/mm), which was already available in the was incorporated into the experiment. Therefore, after the prism, the diode laser beam is expanded by a factor of three by use of two plano-convex lenses in order to fill the diffraction grating. The grating is placed at an angle such that the first order diffraction returns directly back to the prism beamsplitter. Further details on the diffraction grating are discussed in Section 3.4.2. From the beamsplitter, the diode laser beam passes to a mirror and then through an iris. The broadband is diffracted from the grating at a slightly different angle, and hence does not pass through the iris.

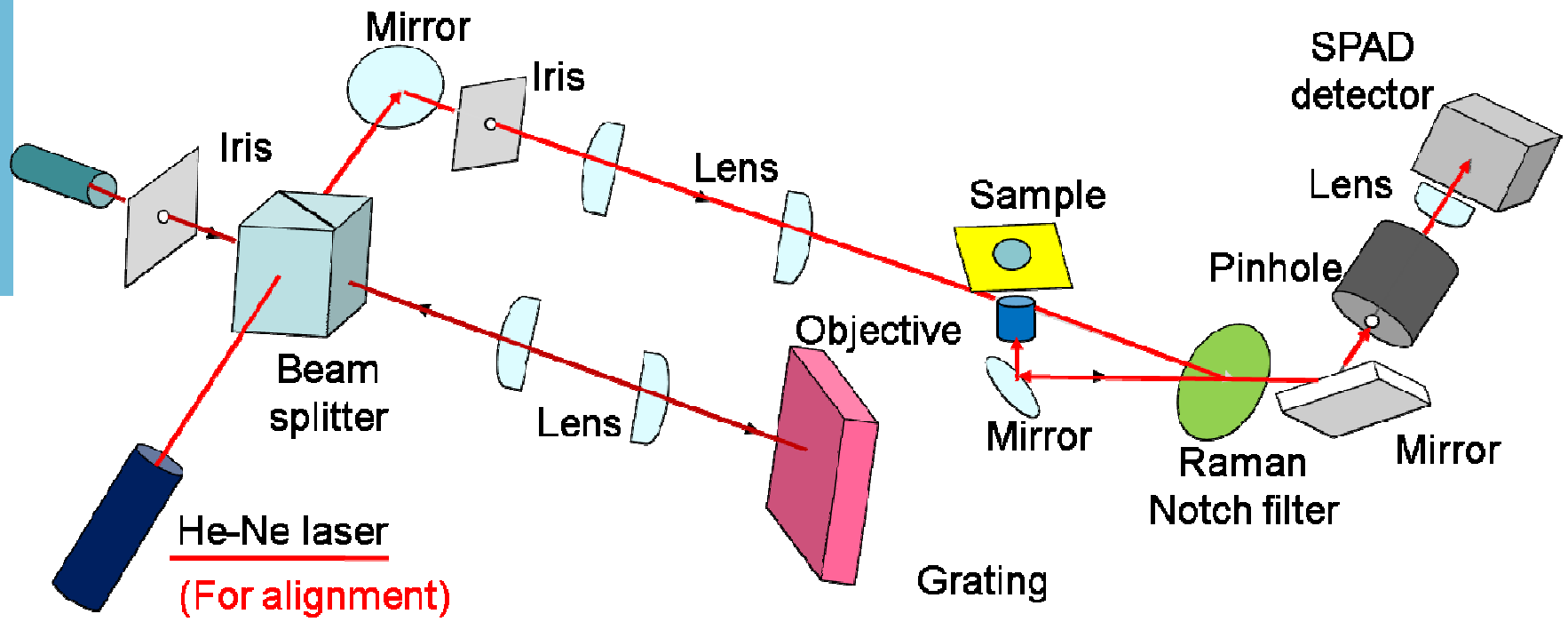

Figure 8 Confocal microscope setup for detection of ZnPc

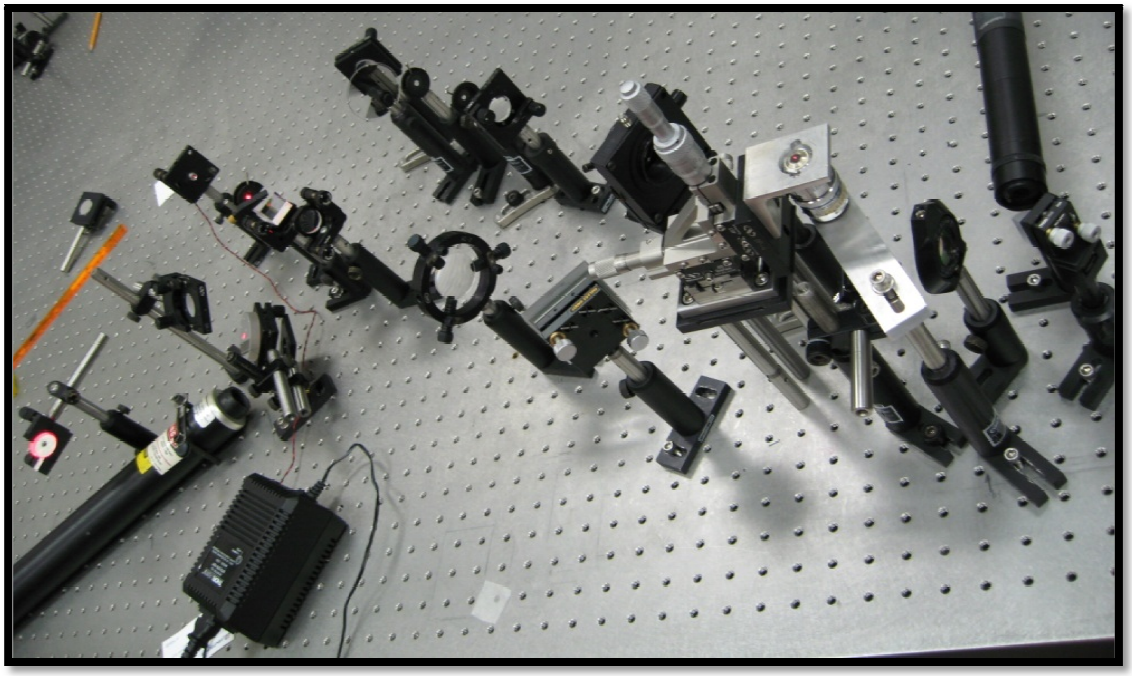

Figure 9 Photo of the setup

The measured spectrum of the diode laser after the diffraction grating is reported later in the chapter.

After the iris, the filtered diode laser beam is expanded and focused prior to entering the microscope. The focusing and expansion of the laser beam was accomplished with the use of two plano-convex lenses, each of diameter 25.4 mm and of focal lengths 50 mm and 100 mm (Newport). The second lens is held within an xyz mount (to adjust the confocal condition, as discussed in Section 3.3) and the position was adjusted so that the beam was focused approximately 60 mm before the Raman notch filter, as discussed below. This filter (Kaiser Optical Systems, Inc., super-notch plus) was custom designed for a center wavelength of 672 nm when used at normal incidence. In the alignment of the instrument, the angle of mounting of the filter had been set so that it would reflect the 667 nm diode laser wavelength towards the microscope objective, while any remaining broadband luminescence would pass

through the Raman notch filter, so that it would not enter the microscope. Further details on the Raman notch filter are discussed in Section 3.4.1.

The diode laser excitation beam then reflects from a mirror to a microscope objective (Nikon CF Plan Achromat 79173), which focuses the beam into the sample solution. This objective was chosen because it was already available in the lab and because it has a high numerical aperture and is well corrected for aberrations (NA 0.85, dry, working distance 0.41–0.45 mm, correction collar for 0.11–0.22 mm coverslip). However, the objective is an older design, i.e., it is not designed for an infinite conjugate but is designed for a 150 mm microscope tube length. Therefore, to achieve tight focusing of the laser, the beam must fill the back aperture of the microscope objective (4 mm diameter), but also the beam must be focused 150 mm prior to the mount of the objective. It is for this reason that the beam is focused 60 mm before the Raman notch filter, as this is 90 mm from the objective mount.

The microscope objective is vertical and mounted in a fixed position. A precision xyz translation stage (Newport 461) holds a mount for the coverslip, so that it may be positioned so that the beam is focused about 50 microns above the top surface of the coverslip, within a drop of sample solution.

The fluorescence from the sample excited by the 667 nm wavelength light is by the same objective and follows the same path to reflect from the mirror back towards the Roman notch filter. It passes through this and comes to a focus 150 mm in path length from the objective. At this point a pinhole is mounted. The pinhole acts as a spatial filter and is confocal to the focus of the laser beam within the drop of sample. Scattered laser light is blocked by the Raman notch filter, as it is reflected back towards the laser. Thus the fluorescence light is separated by the Roman notch filter from residual excitation light. Also, the pinhole helps to eliminate the scattered laser radiation as it only passes light that originates from nearby the laser focus. For example, if there is weak fluorescence from the glass coverslip, this may pass

through the Raman notch filter, but it will be blocked by the pinhole.

Following the pinhole is a tube, which contains a bandpass filter to further suppress background, as discussed in Section 2.4. Then, at a distance of 180 mm from the pinhole is an achromat lens of focal length 19 mm (Thorlabs, AC127-019-A1), which focuses the fluorescence onto the 150 micron-diameter active area of the SPAD. Zemax optical design software was used to select the distances between optical components to minimize aberrations, while achieving focusing as tight as possible on the SPAD. The exact alignment of the components, including the pinhole and the SPAD, was made using the HeNe laser, as described in the following section.

3.2 Optical alignment

For alignment, the collinear HeNe laser beam at 632.8 nm is turned on. This partially reflects from the Raman notch filter and into the microscope objective. The coverslip is raised so that the top surface is at the focus of the laser to generate a reflected beam. A fraction of the HeNe beam then reflects from the coverslip surface back to the Raman notch filter. A fraction of this is then transmitted by the Raman notch filter and is focused onto the pinhole, which is then aligned so as to pass the HeNe beam. The beam also passes through the bandpass filter and on to the SPAD, which is mounted on a precision xyz translation stage. The HeNe beam can then be further attenuated for initial alignment of the SPAD.

Next, with the HeNe turned off, the coverslip is lowered and a moderately concentrated dye solution is placed on the coverslip, so that the alignment can be adjusted using the fluorescence signal. The SPAD position is adjusted first.

A simple photon-counting Labview program (written by CLA graduate research assistant Jason King) is used to monitor the photon count rate while moving the detector along each individual translation axis. Once the maximum rate per axis is found, the detector is translated along that axis in each direction until the count rate drops to half the maximum, thereby defining the focal spot diameter for that axis. The procedure is iteratively performed for all three axes until the determined best position does not change appreciably. Note that along the z-axis (in the direction of beam propagation) the focused intensity does not change rapidly over short distances as it does along x and y. (In later experiments, SPAD alignment was accomplished with an automated system developed by CLA postdoctoral research associate Dr. Brian Canfield. This uses a LabView program to monitor the count rate as it controls three motorized actuators to adjust the SPAD position.)

3.3 Optimizing the beam focus for the confocal condition

As mentioned in chapter II, it is crucial to meet the confocal condition in order to

achieve detection at the single-molecule level. The placement of the objective lens and the pinhole together define a small region in the object space from which fluorescence light is most efficiently collected. This is shown as the dashed oval in Figure 10. The laser beam is focused to a waist shown in red in the figure. The excitation volume is defined by the overlap of the focused laser and the region from which light is efficiently collected through the pinhole. The confocal condition occurs when the center of the laser beam focus is the same as the center of this collection region in object space. If the center of the laser focus is slightly offset, then the fluorescence signal is not so strong, and also the size of the volume that is excited and from which light is collected is larger. The top picture in Figure 10 shows the where the laser waist is misaligned laterally and the bottom picture shows axial misalignment.

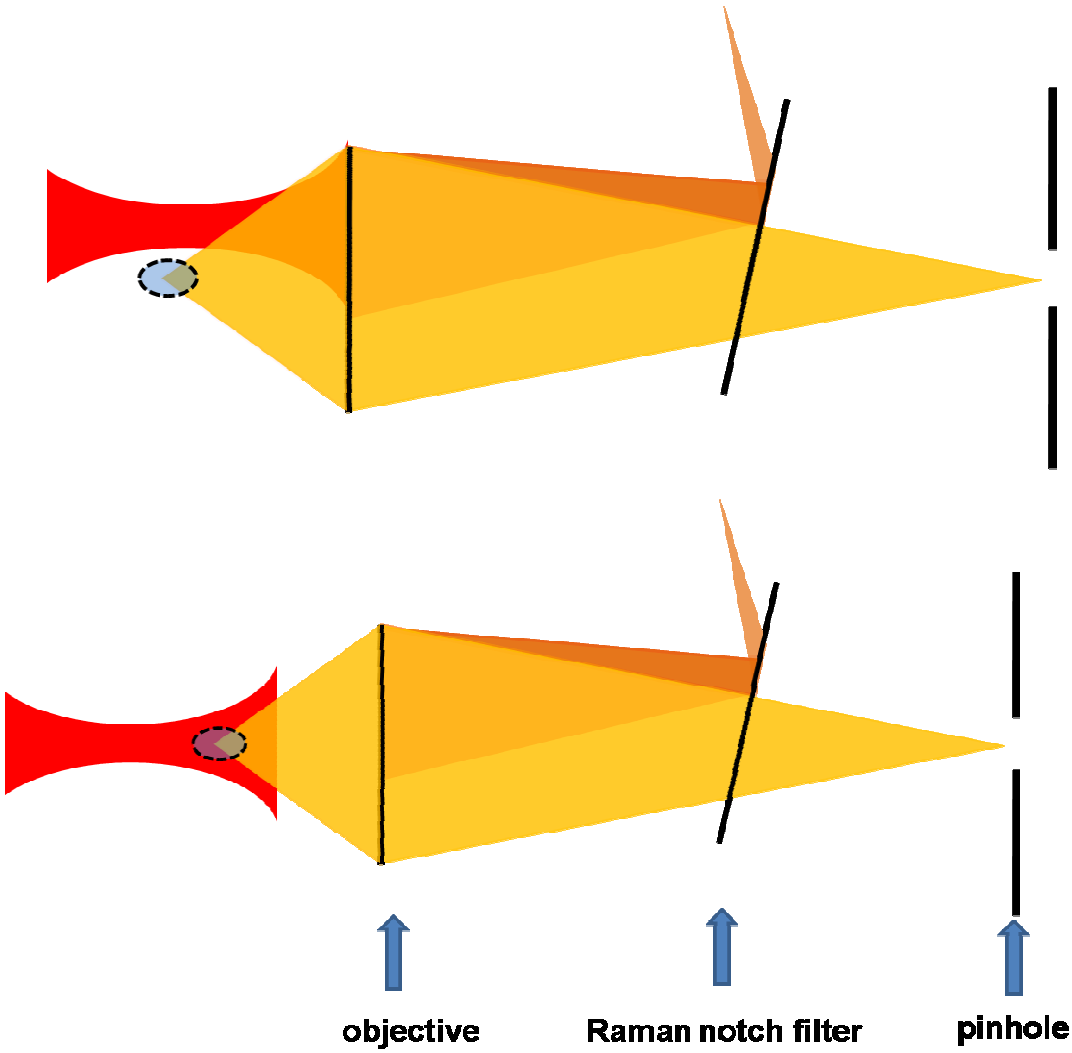

Figure 10 Confocal excitation volume showing misalignment of the laser focus

In order to measure an ACF with a reasonably large amplitude and smooth shape with small width, there must be a small number of molecules in the excitation volume and the signal-to-noise must be good and approaching that needed to observe photon bursts from single molecules. The amplitude of the ACF of the fluorescence fluctuations has a close relation with the mean number of the fluorescence molecules in the excitation volume. It provides information on the number densities of the fluorescent molecules. Simply speaking, the amplitude of the ACF increases when there is a smaller number of fluorescence molecules in the excitation volume as this leads to greater relative fluctuations. Therefore if we want the magnitude of the ACF to be about 2 or higher we need to make the size of the excitation volume small by correctly adjusting the confocal condition.

Generally, the optical alignment is not exactly at the confocal condition when the experiment is first set up and it is necessary to use the lens in Figure 11 shown below to adjust the position of the laser beam focus in the solution. In this figure, the lens is moved in both the z direction and the x,y direction. As shown in the figure, if the lens is moved backward from (a) to (b) along the z axis, the focus of the laser beam will move further from the objective in the solution (i.e., moved from (a) to (b)), and if the lens is moved in the x,y plane, it will make the laser beam focus move around in the solution at the same depth, as shown at point (c).

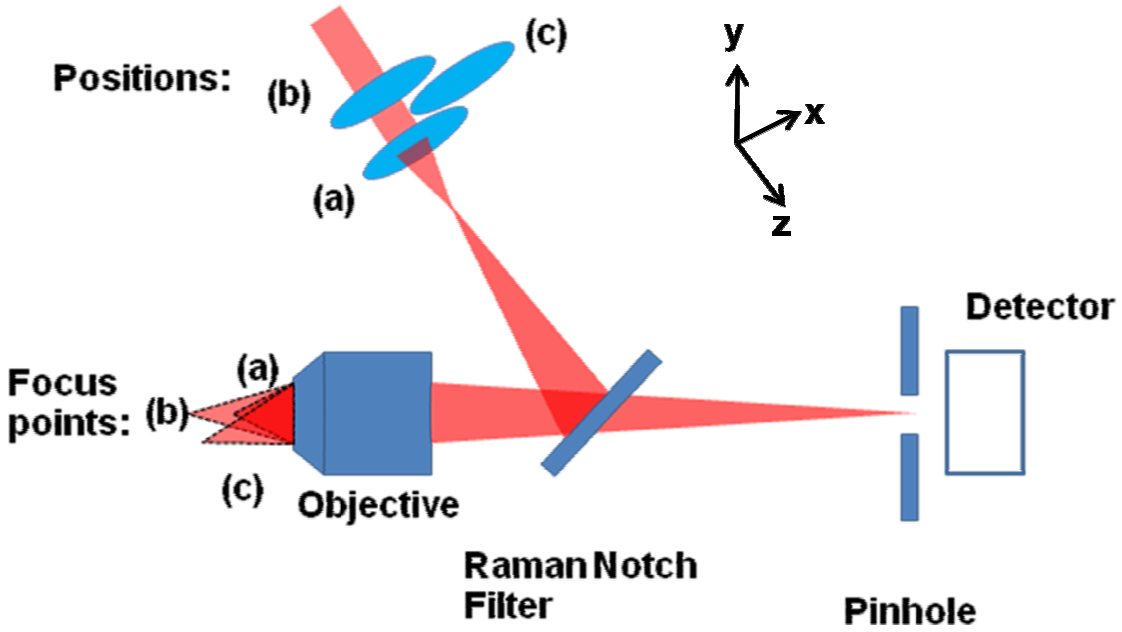

Figure 11 Optimization of the lens position to achieve the confocal condition

Figures 12 and 13 show how optimization of the lens affects the ACF and photon bursts as the confocal condition is adjusted. These adjustments are made by use of a solution of Alexa 660 solution with a concentration of 180 nM, with the diode laser power attenuated to 30 μW for all measurements, and with fluorescence collected for 100 s. When it's not in an ideal confocal position, the ACF width will be wider as seen in Figure 12. Only when the system achieves a relatively better confocal condition will we achieve high photon bursts and a good shape for the ACF, as seen in Figure 13.

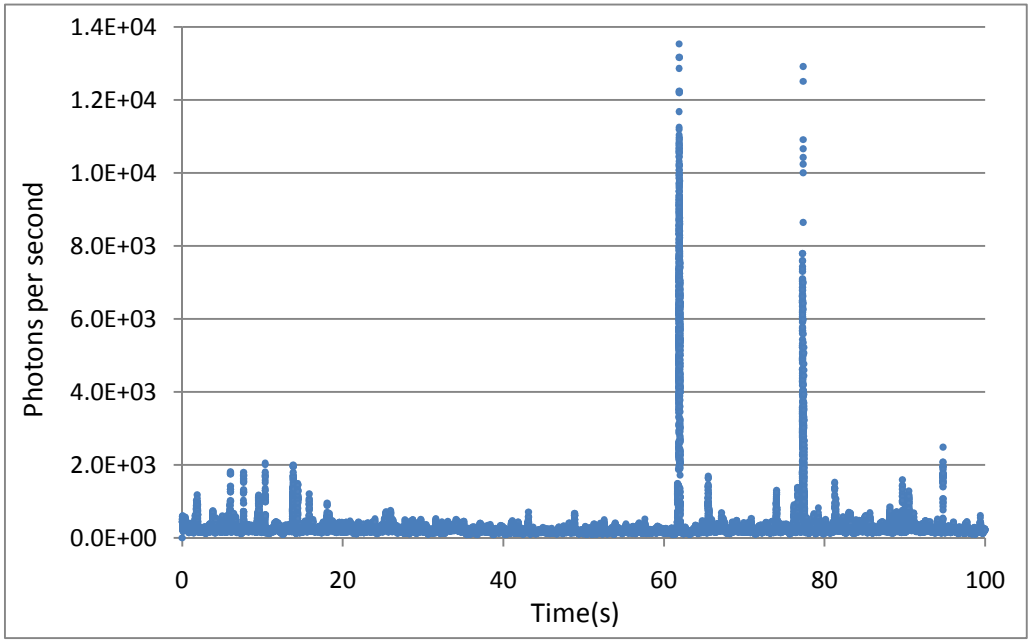

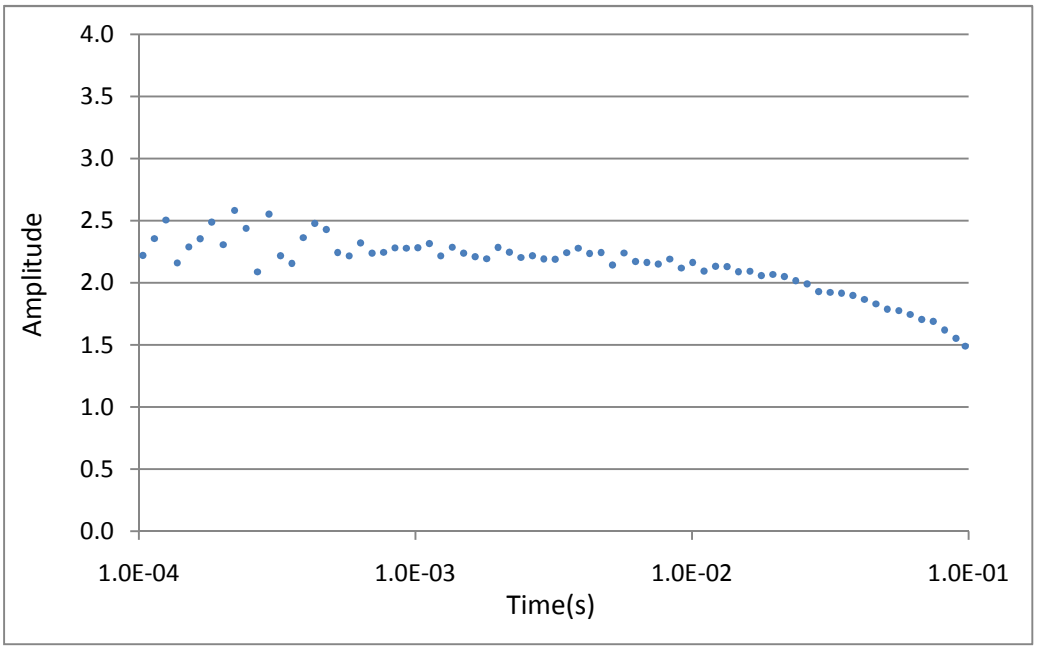

Figure 12 Photon bursts and autocorrelation curve of Alexa 660 at non-optimized confocal condition

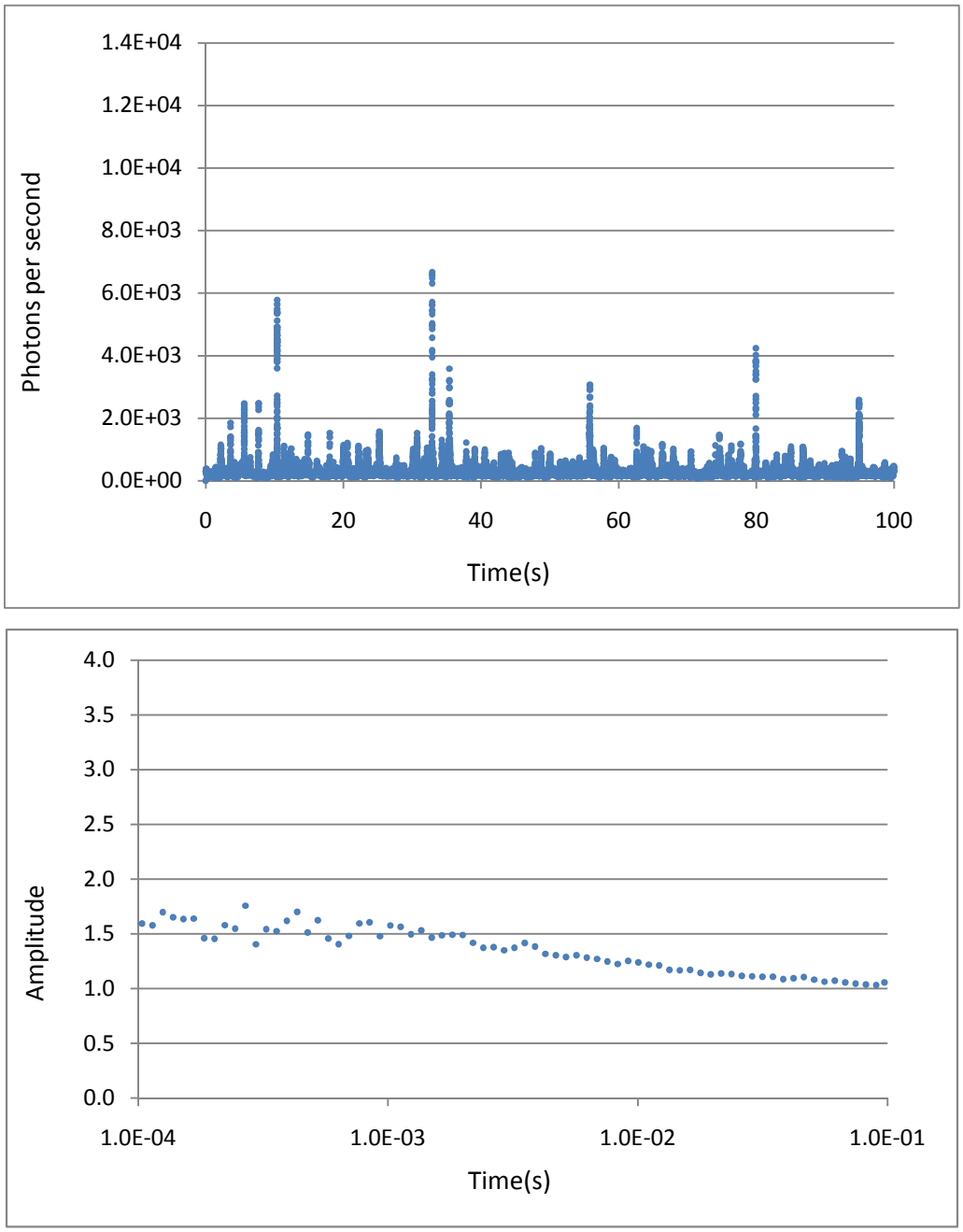

Figure 13 Photon bursts and autocorrelation curve of Alexa 660 at improved confocal condition

3.4 Optical components

3.4.1 Angle-tuned Raman notch filter

Prior to use of the Raman notch filter in the experimental set up, calibration measurements were made with a spectrophotometer (GenTech TU-1901) to determine its reflection as a function of wavelength and angle. An experiment was performed to find the angle of alignment for the filter for it to work at the diode laser wavelength of 667 nm.

The filter was placed at zero incidence angle and the optical density was measured as a function of wavelength. Figure 14 shows that at normal incidence angle the filter reflects light at a wavelength of 672 nm.

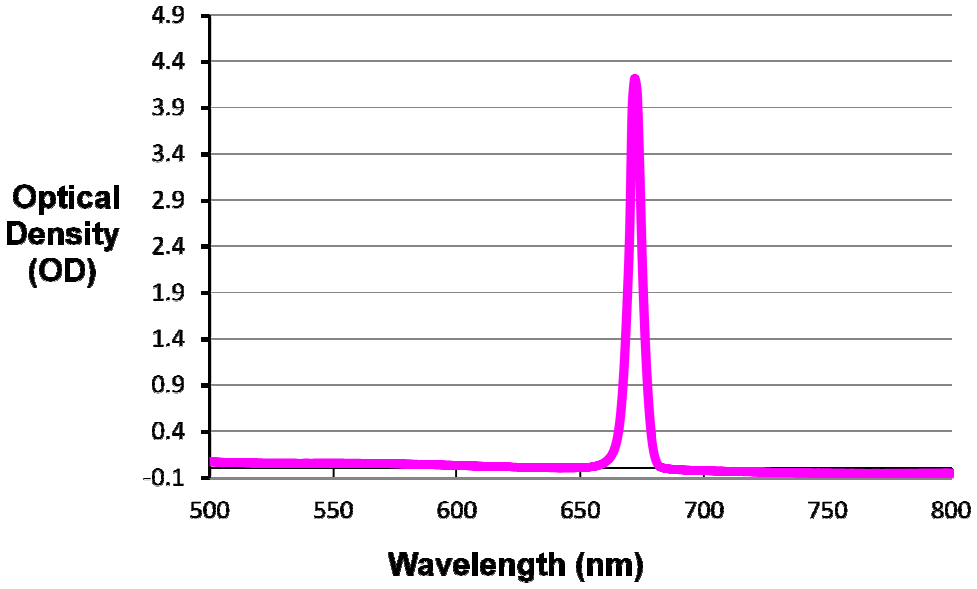

Figure 14 Optical density due to reflection of the Raman notch filter versus wavelength

Figure 15 shows how transmission of light changes as a function of the angle of incidence. The wavelength was selected to be the same as the diode laser at 667 nm and the filter was mounted onto a rotation stage, so that the transmission was measured every two degrees. This sharp notch here shows where the Raman notch filter reflects all the excitation light. Consequently the filter must be mounted in the experimental setup at 18 degrees. The transmission of the Raman notch filter when aligned at this angle is included in Figure 3.

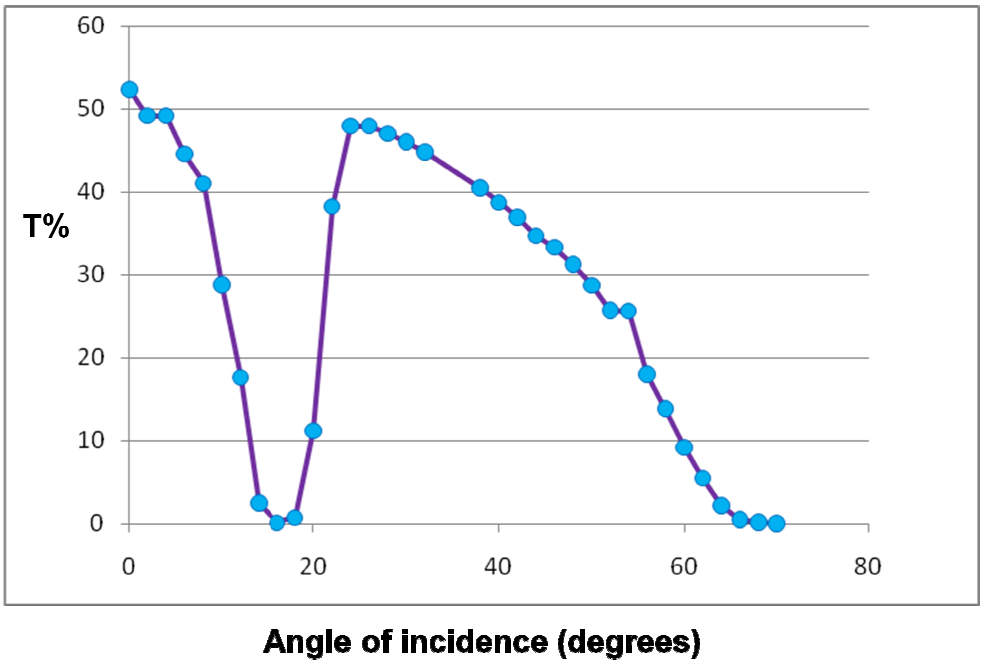

Figure 15 Transmission of the Raman notch filter at 667 nm wavelength as a function of angle

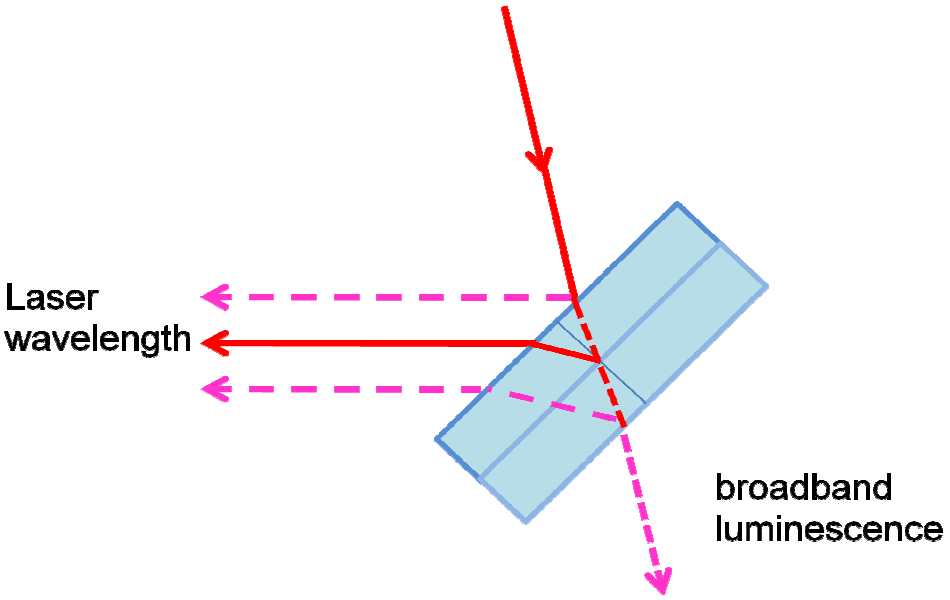

Figure 16 Use of the Raman notch filter in the experimental setup

Figure 16 illustrates the use of the Raman notch filter in the experimental setup. The filter itself is sandwiched between two glass plates. The laser wavelength reflects from the filter towards the microscope objective.

It is intended that the broadband luminescence from the diode laser would pass through the Raman notch filter and not enter the microscope. Figure 17 shows the spectrum of the light that is transmitted through the Raman notch filter, as measured with a fiber-optically coupled spectrometer (Ocean Optics, model USB4000). However, there is some Fresnel reflection of these wavelengths from the interfaces the glass plates. In particular, the green line in Figure 17 shows the wavelength of light peaks at 672.73 nm. In initial setups of the experiment it was found that this Fresnel reflection of light to the sample (measured to be 130 nW with a power meter) resulted in Rayleigh scattered light from the sample, which became a major source background. The peak wavelength of this leaking light is at 672.3 nm, as shown by the green line in Figure 17.

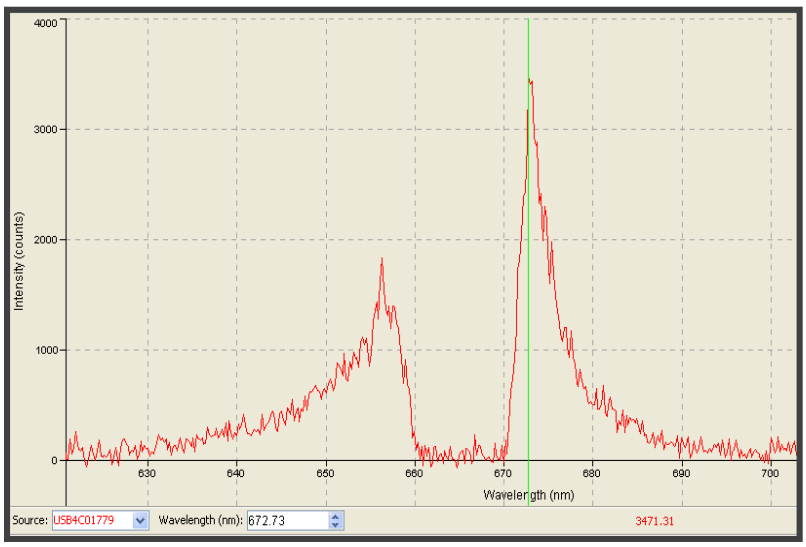

Figure 17 Broadband luminescence after the Raman notch filer

It was thereby determined that the Raman notch filter by itself was not sufficient to eliminate the broadband luminescence from the diode laser. A laser line interference filter at 660 nm available in the lab was used in an attempt to eliminate the background from the broadband luminescence. However, the spectral width of this filter was such that it could not eliminate all of the broadband diode laser luminescence without also cutting into the emission spectrum of the phthalocyanine dye. Hence a diffraction grating was used, as described in the following section.

3.4.2 Diffraction grating for elimination of broadband luminescence

A diffraction grating was set up to act like a monochromator to pass the laser wavelength but block nearby wavelengths, which are due to weak broadband luminescence collinear with the diode laser beam. In Figure 8, it is seen that the diffraction grating is placed so that the first diffraction order (m = 1) passes back the incident beam path. The grating was a holographic grating available in the lab with 1200 lines/mm, i.e., the line spacing is $d = 8.3 \times 10^{-7}$ m. When a plane wave of wavelength λ is incident on the grating at an angle of incidence θ_i, light is diffracted from the grating at an angles θ_m given by

$$d \cdot (\sin\theta_m + \sin\theta_i) = m \cdot \lambda, \qquad (1)$$

where m is the order of diffraction. For λ = 667 nm, there is only one order, with θ_i = θ_m = 26.3°, hence the laser light is diffracted back to the source when the grating is tilted at this angle. The broadband luminescence from the diode laser at nearby wavelengths is diffracted at slightly different angles so that this does not pass through the iris. Hence after this iris, the beam transmitted to the microscope is composed of a selectable narrow band of wavelengths, as seen in Figure 18 which is measured with the Ocean Optics USB-4000 spectrometer. The spectral width of this beam is determined by the area of illumination of the grating, and thus the beam from the diode is expanded before it reflects from the grating.

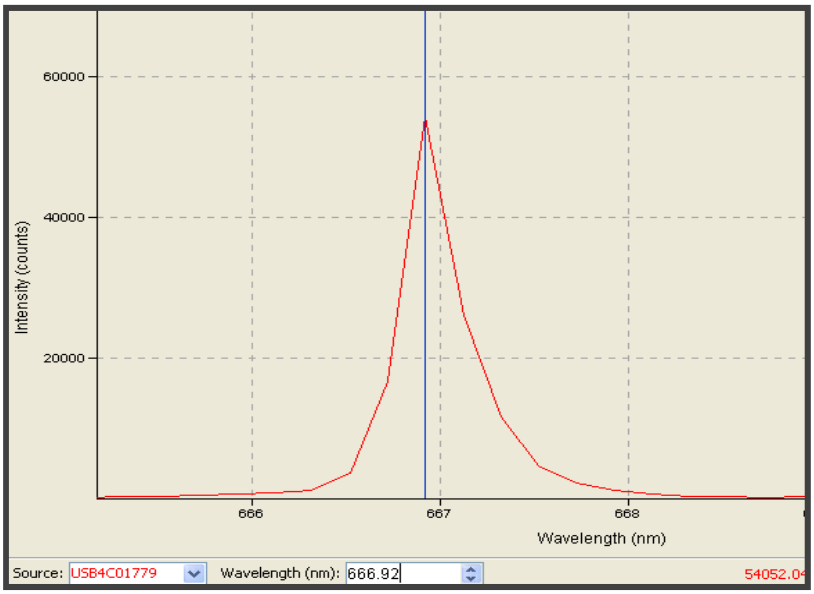

Figure 18 Spectrum of the laser beam after the diffraction grating and Raman notch filter

3.5 Data collection and processing

The collected fluorescence is focused onto the active area of the SPAD detector, which converts the detected photons into transistor-transistor-logic (TTL) pulses [15]. These are input to a counter-timer card (PCI-6602, National Instruments Austin, TX), which works like a watch or chronometer to give the timestamp (or time-of-arrival) of each photon detected by the SPAD. The PCI card is inside a PC, which has a homemade counter program written in LabView (by Jason King). Also, there is a program written in LabView (by Dr. Lloyd Davis) for calculating the ACF [1]. In the experiment, the SPAD was connected to the PCI card and the time delays between pulses from pairs of photons were histogrammed within the software to form the The software enables rendering of separate time-tagged photon traces with a resolution of 12.5 ns for one or two detection channels. The internal 80-MHz clock of the card was used as the time base.

3.6 Autocorrelation function

At equilibrium, fluorescent molecules moving through the confocal microscope volume and/or undergoing transitions between different states yield temporal fluctuations in the fluorescence signal. The ACF of the fluorescence signal, g(τ), which measures the average duration of the fluorescence fluctuations, decays with time delay, τ. The magnitude of the ACF provides information on the number densities of the different fluorescent species in the sample. In HTS the number densities of fluorescent molecules bound to a target and free in solution may be measured from the ACF [16].

The ACF represents the correlation coefficient between the intensity at time t, I(t), the intensity at a time t+ τ, I(t+ τ). The ACF can be expressed as:

$$g(\tau) = \frac{\sum_{i=0}^{M-m} I(i\Delta t)I(i\Delta t+m\Delta t)}{<I>^2(M-m)}, \qquad (2)$$

where m is an integer multiple of a time interval, Δt such that τ = mΔt (where 0 ≤ m < M). I(t) is the time-resolved fluorescence intensity with M + 1 data points spanning from t = 0 to t = MΔt. <I> is the mean intensity over all values of t.

3.7 Afterpulsing and its correction in FCS

Afterpulsing arises from trapped charges within the detector. The origin of this effect depends on the detector and on the working environment**.** Each real signal pulse has a probability to be followed by an afterpulse at a later time. This effect will cause a peak in the early time period of the acquired ACF and thus will make it difficult to determine the average number of molecules in the detection volume and the diffusion constant of the molecules. Moreover, it will greatly limit the minimum dwell time and detection sensitivity.

Generally, a probabilistic approach is used to form models which explain this phenomenon. Each single event detected at time t has a probability $\alpha(\tau)$ of being followed by an afterpulse at time t+τ. The afterpulsing probability $\alpha(\tau)$ is determined by properties such as material defects, which can lead to trapped charges, and the particular operating conditions.

With the presence of afterpulsing, the measured normalized ACF will be

$$g'(\tau) = g(\tau) + \frac{\Delta t}{\mu}\alpha(\tau) \ , \qquad (4)$$

where μ is the mean number of counts during each time interval Δt and μ <<1.

One can get $\alpha(\tau)$ from a separate calibration measurement of the ACF of a non-non-correlated light source. As the non-correlated source is expected to have $g(\tau)$ = 1, the $\Delta t\alpha(\tau)$ term can be obtained from

$$g'(\tau) = 1 + \frac{\Delta t}{\langle i \rangle}\alpha(\tau)\,, \qquad \tau \neq 0 \quad , \qquad (5)$$

where $\langle i \rangle$ is the mean number of counts during the dwell time for the calibration measurement [16].

Before the experiments, the afterpulsing pattern of the SPAD is measured and saved in an Excel file, where it is fitted to a two-exponential decay, as explained below. information yields $\alpha(\tau)$, which is then used by the Labview program to eliminate distortion of the ACF due to afterpulsing as the ACF is accumulated and graphed.

To make the correction, first the afterpulsing pattern is obtained by measuring the scattered light in pure water with the bandpass filter removed and the power of the laser source adjusted to give a photon count rate of about 10^5 s^{-1}. Typically the experiment is performed in pure water for 100 sec which is the same time we collect the fluorescence from the sample. Then this afterpulsing pattern information is used by the program to calculate $\alpha(\tau)$ for use in Eqn (5). The decay time of $\alpha(\tau)$ is on the order of 10^{-6} s, as shown in Figure 19. Parameters are acquired from curve fitting the measured afterpulsing ACF to a two-exponential function by use of the Solver in Excel and then the curve fit yields $\alpha(\tau)$.

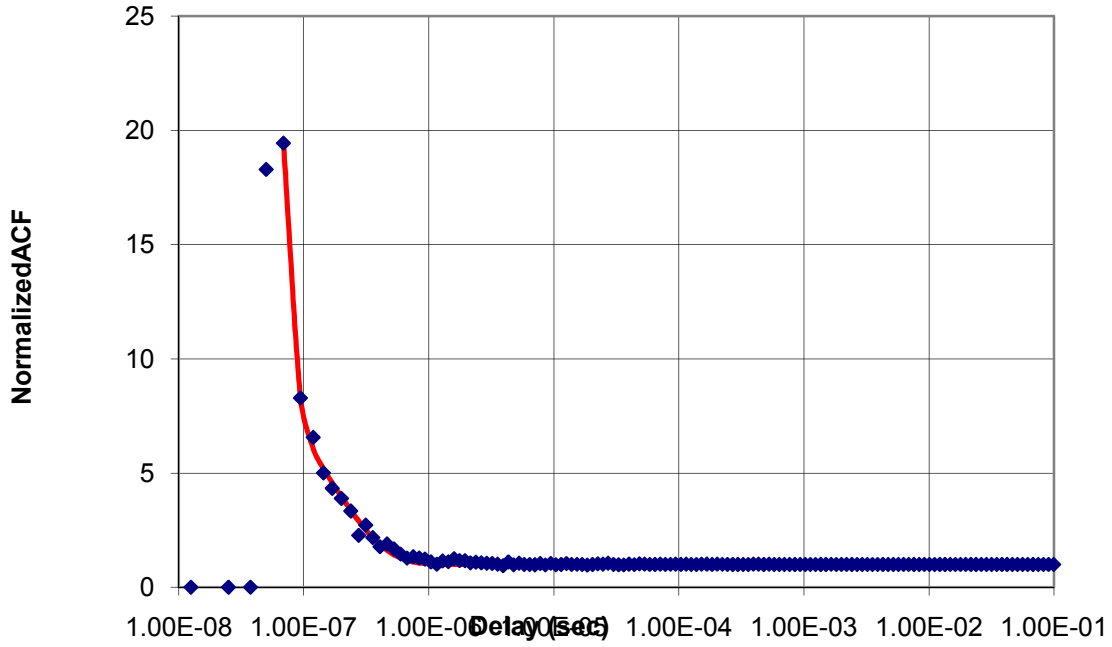

Figure 19 Afterpulsing correction in Excel.

Another approach to avoid the effects of afterpulsing is to split the fluorescence onto two separate detectors in a so-called Hanbury-Brown and Twiss setup and to calculate the cross correlation function of the two signals. This will also circumvent the dead time of the SPAD, but it requires two detectors. The equation used here is:

$$g(\tau) = \frac{\langle I_1(t) I_2(t+\tau) \rangle}{\langle I_1(t) \rangle \langle I_2(t+\tau) \rangle}, \qquad (6)$$

where I_1 and I_2 are the signals at each of the detectors.

Chapter IV

Zn-Phthalocyanine detection measurements

4.1 Sample preparation

The ZnPc stock solution was provide by Dr. Steven A. Soper from Louisiana State University. The compound ZnPc was dissolved in ethanol. The Alexa 660 was purchased from Invitrogen (http://www.invitrogen.com/site/us/en/home/brands/Molecular-Probes.html) and was dissolved in ultrapure water (Barnstead Nanopure UV). The two solutions were prepared separately by serial dilution of stock solutions into different amounts of solvent (water or ethanol) to give different concentrations (0.188 nM, 1.88 nM, 18.8 nM, and 188 nM), as seen in Table 1. The concentrations of the stock solutions were determined by measuring the absorption in a spectrophotometer (GenTech TU-1901). Then, with use of the known extinction coefficient, the stock solution concentration can be calculated from the Beer-Lambert Law:

$$A = \varepsilon\, l\, c, \qquad (7)$$

where A is the measured absorbance; ε is the known extinction coefficient (for ZnPc, ε= 2.85x10^5 M^{-1} cm^{-1}; for Alexa 660, ε= 1.32x10^5 M^{-1} cm^{-1}), l is the path length (l=1 cm); and c is the concentration to be determined.

After the stock solutions were prepared, the series of four dilute solutions were obtained by serial dilution by a known factor (i.e., by addition of 100 microliters of solution to 900 microliters of solvent for a 10-fold dilution) until the fluorescence counts are barely above that of water. Typically, 1 ml of each sample was stored for later use in a closed vial.

4.2 Concentration measurements

Measurements of the fluorescence count rate were carried out using a series of sample solutions of varying concentrations of ZnPc. The measured count rate data are shown in Table 1 and the curve of the concentration as a function of count rate is plotted in a log-log scale in Figure 20.

For the experiment for detection at the single-molecule level, a sample of approximately 50 microliters of nanomolar concentration Alexa 660 or ZnPc dye solution was deposited with a micropipette onto a new clean glass coverslip. All experiments are performed at ambient temperature. In order to focus the laser into the solution, the sample was first positioned so that the reflection from the top surface of the coverslip was focused at the pinhole and then the micrometer was adjusted to move the sample down closer to the high-NA objective by 50 μm.

In Figure 20, an ethanol background of 223.7 s^{-1} was subtracted. The count rate has a linear relation with the concentration in the comparatively dilute solution. When the concentration goes beyond about 100 nM, the linearity breaks down. This is probably due to quenching of the fluorescence of the dye due to aggregation. Note that there is only one error bar visible in Figure 18, because the error bars for the other four measurements are too small to be seen.

For this series of experiments, a peak in the ACF was not achieved because the confocal condition was not well aligned. In Section 4.2 the setup is realigned and the ACF curve is plotted.

Table 1 Determination of count rates from measurement results

Concentration (nM)	1880	188	18.8	1.88	0.188
Total counts	577712	364224	89487	21478	13758
Time (s)	60	60	60	60	60
Total count rate (s^{-1})	9629	6070	1491	358	229
Count rate with background subtracted (s^{-1})	9404	5846	1268	134	5.6
Error (s^{-1})	13.2	10.8	6.3	4.6	4.3

Background rate=223.7±3.9s^{-1}

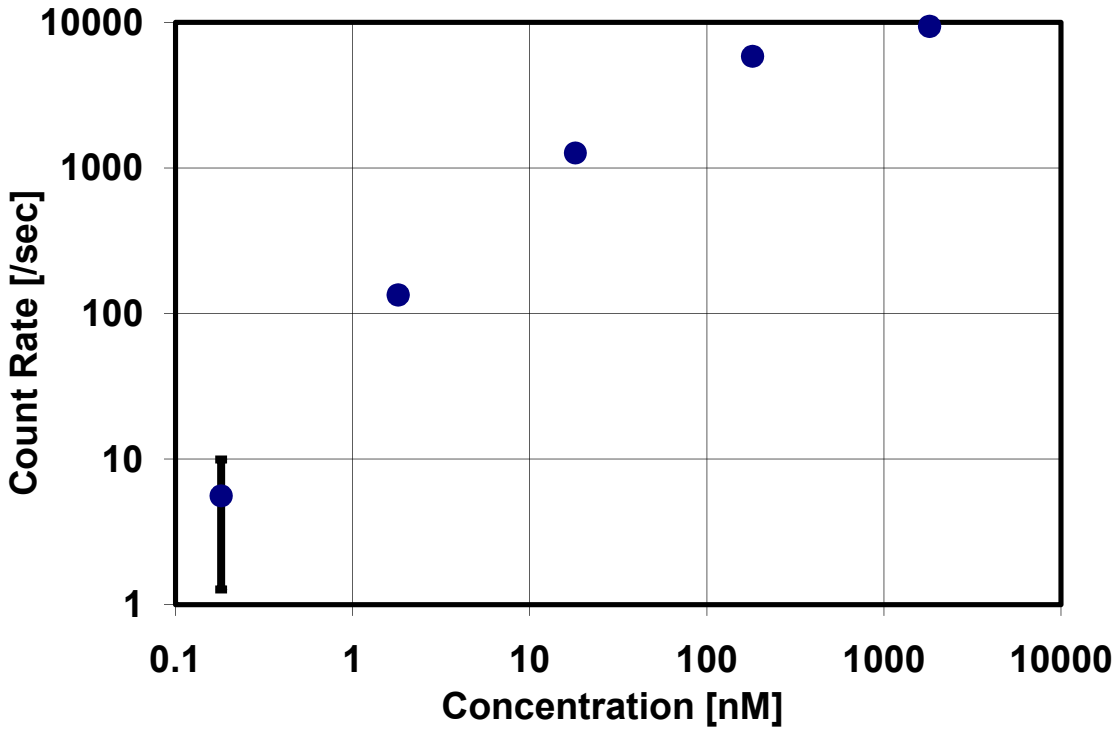

Figure 20 Count rate versus concentration for ZnPc dye in ethanol

4.3 Autocorrelation analysis

After the experimental setup was carefully realigned, the single-molecule detection experiment was carried out using both Alex 660 and ZnPc dyes. Two of the results, which use 10 pM and 1 nM ZnPc dye in ethanol with 30 μW diode laser power are shown below in Figures 21-24.

In Figure 21, photon bursts are seen during the 100 sec collection time. The amplitude of the bursts is on the order of 1000 counts per second and the background is around 150 counts per second. The low background proves that the broadband luminescence has been eliminated and that Raman scatter from the solvent has also been effectively blocked.

In Figure 22, the ACF is plotted. The amplitude of the ACF is relatively small compared to that seen in other FCS experiments because the signal to background is still relatively weak. These results were obtained with a bandpass filter that blocks some of the fluorescence (light blue curve in Figure 3) and it should be possible to achieve greater signal by replacing this filter (e.g., with that of the yellow curve in Figure 3). Also, the width of the ACF is slightly wide which indicates that the confocal volume is relatively large and hence it should be possible to improve the confocal condition to get a better focus.

In Figure 23, it is obvious that the 1 nM solution has many more photon bursts than that with 10 pM. The bursts are overlapping so the maximum photon amplitude reaches ~10^4 count/s. The data also illustrates why it is not possible to get a large peak in the ACF from a concentrated solution. The ACF amplitude increases when molecules giving fluorescence cross the excitation volume decreases. Therefore when there are too many photon bursts, the amplitude of the ACF won't be high.

In Figure 24, besides the autocorrelation peak, there is a large peak in the early time

period. This is basically due to the triplet state of the dye molecule. When molecules cross to the triplet state, they don't give fluorescence, but instead, they decay by phosphorescence and make changes in the fluorescence fluctuations and thus changes in the shape of the ACF.

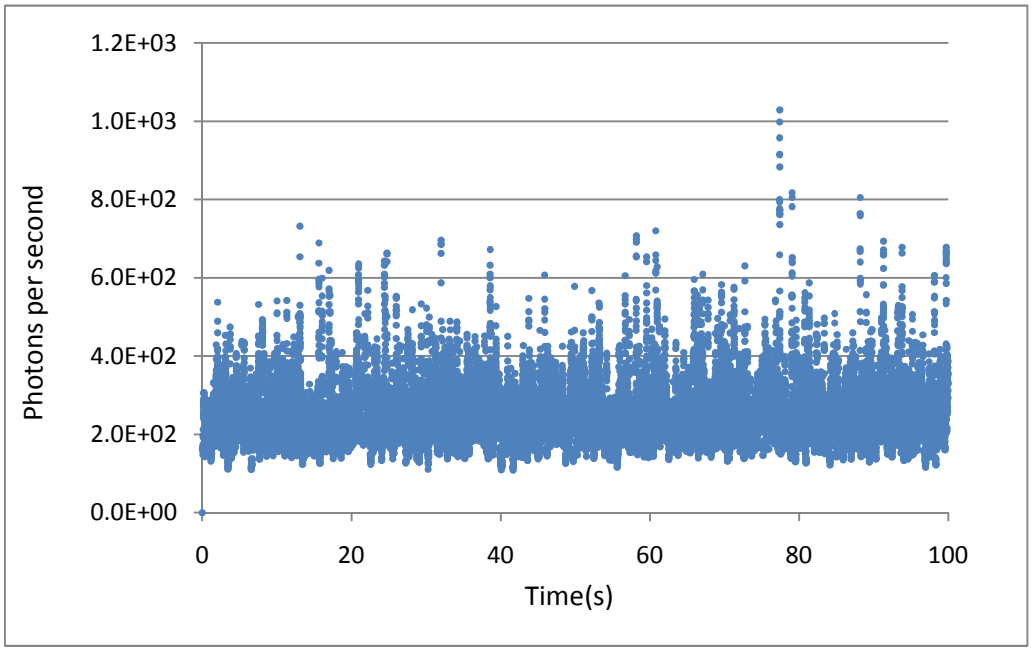

Figure 21 Photon bursts of ZnPc dyes

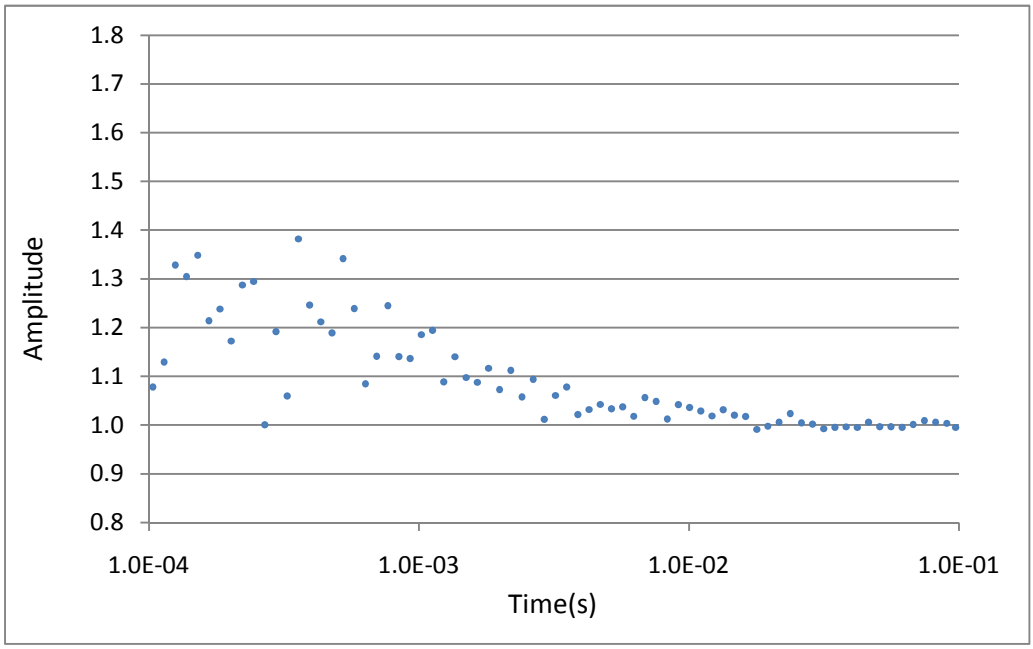

Figure 22 Autocorrelation curve of ZnPc dyes

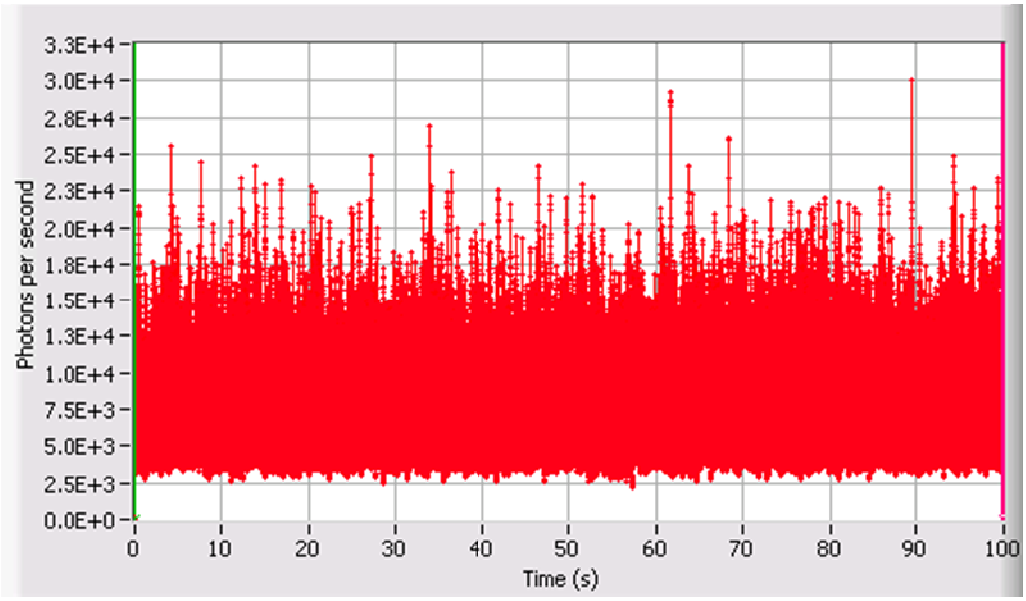

Figure 23 Photon bursts of ZnPc dyes with more concentrated solution

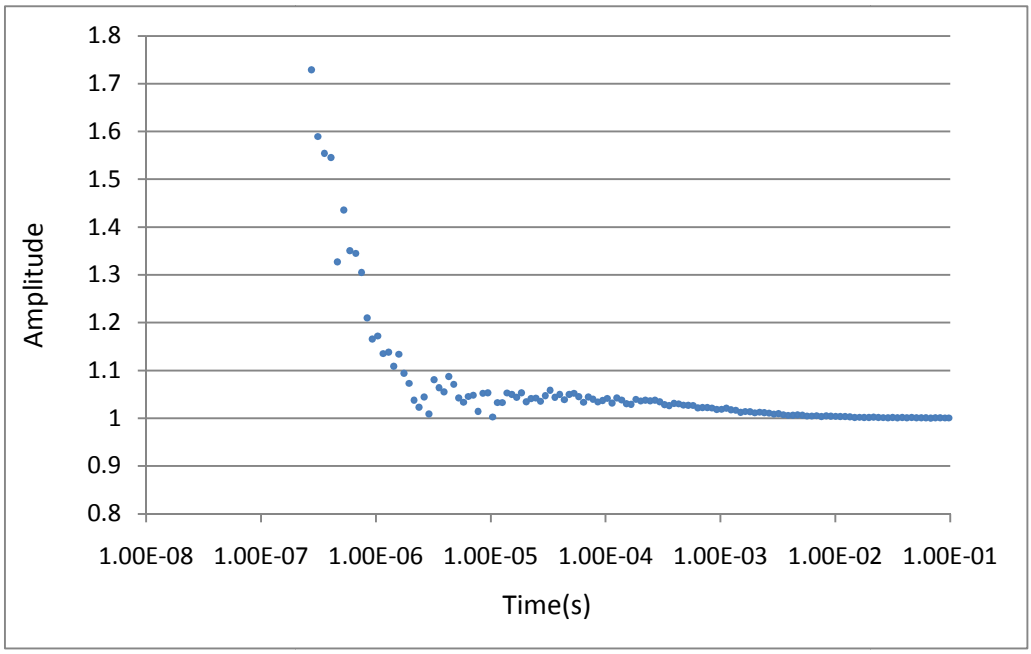

Figure 24 Autocorrelation curve of ZnPc dyes with more concentratedsolution

Chapter V

Conclusion and ongoing work

A low-cost instrument has been built for ultrasensitive detection of deep-red and near-infrared fluorophores To suppress the broadband luminescence from the diode laser, a diffraction grating is placed in the laser beam path, before the beam is passed into the system. This greatly improves the signal-to-noise. Also, because the Stokes shift of ZnPc is small, a Raman notch filter was used to provide the capability for efficient fluorescence throughput for higher signal-to-noise. However, the instrument also included a bandpass filter, which reduced background due to Raman scatter from solvent molecules, but which unfortunately also reduced the fluorescence signal. Nevertheless, the sensitivity for detection of ZnPc in ethanol has been successfully lowered down to ~0.2 nM from a measure of the photon counts and to ~10 pM from the autocorrelation function of the photons.

For ongoing work, experiments will be conducted with a bandpass filter that provides more efficient throughput of fluorescece, such as that shown by the yellow curve in Figure 3. Also, the width of the ACFs in Figures 22 and 24 indicates that the diode laser beam is not tightly focused in the confocal volume and that the beam needs to be shaped to a Gaussian intensity profile prior to the experiment. In past work, an attempt was made to pass the beam through a single mode fiber but the transmitted power was not strong enough. However, in recent ongoing work, the beam has been focused through a pinhole which acts as a spatial filter to produce a nice circular Gaussian profile. This is expected to enable improved signal-to-background in ongoing single-molecule detection experiments.

Also, in future work, the instrument will be used for near-ir fluorescence detection applications within polymer microfluidic devices and will be adapted to parallelized

measurements with the use of an electron-multiplying CCD detector. These are all important steps for the final realization of the platform for high throghput screening, and they should also find application to other biomedical technologies.

References

[1]. L.M. Davis, P.E. Williams, D.A. Ball, E.D. Matayoshi, and K.M. Swift, "Data reduction methods for application of fluorescence correlation spectroscopy to pharmaceutical drug discovery," *Current Pharmaceutical Biotechnology* 4, 451-462 (2003); 5, 481-481 (2004).

[2]. E.B. Shera, N.K. Seitzinger, L.M. Davis, R.A. Keller, and S.A. Soper, "Detection of single fluorescent molecules," *Chemical Physics Letters* 174 (6), 553-557 (1990).

[3]. Hamed Shadpour and Steven A. Soper, "Two-Dimensional Electrophoretic Separation of Proteins Using Poly (methyl methacrylate) Microchips", *Analytical. Chemistry.* 78 (11), 3519–3527 (2006).

[4]. Lloyd M. Davis and Guoqing Shen, "Accounting for Triplet and Saturation Effects in FCS Measurements", *Current Pharmaceutical Biotechnology,* 7, 287-301 (2006).

[5]. Elliot L. Elson, "Fluorescence Correlation Spectroscopy I. Conceptual Basis and Theory," *Biopolymers*, 13, 1-27 (1974).

[6]. L.M. Davis, D. A. Ball, P. E. Williams, K. M. Swift, and E. D. Matayoshi, "Dealing with reduced data acquisition times in fluorescence correlation spectroscopy (FCS) for high-throughput screening (HTS) applications," *Proc. SPIE: Microarrays and Combinatorial Technologies for Biomedical Applications: Design, Fabrication, and Analysis, D. V. Nicolau and R. Raghavachari, eds.,* 4966, 117-128 (2003).

[7]. Gustav Persson, Per Thyberg, and Jerker Widengren "Modulated Fluorescence Correlation Spectroscopy with Complete Time Range Information" *Biophysical Journal* 94, 977 – 985 (2008).

[8]. Steven A. Soper and Benjamin L. Legendre, JR. "Single-Molecule Detection the Near-IR Using Continuous-Wave Diode Laser Excitation with an

Avalanche Photon Detector", *Applied Spectroscopy*, Volume 52, Number 1, (1998).

[9]. Wiki; "Stokes shifts", http://en.wikipedia.org/wiki/Stokes_shift, (2009).

[10].Xinzhan Peng, Daniel R. Draney, "Phthalocyanine dye as an extremely photostable and highly fluorescent near-infrared labeling reagent" *SPIE* Volume 6097, 60970E, (2006).

[11].Vera T. Verdree & Serhii Pakhomov & Guifa Su & Michael W. Allen & Amber C. Countryman & Robert P. Hammer & Steven A. Soper, "Water Soluble Metallo-Phthalocyanines: The Role of the Functional Groups on the Spectral and Photophysical Properties" *Journal Fluorescence*, 17:547–563 DOI 10.1007/s10895-007-0210-4 (2007).

[12].A. Spinelli and L. M. Davis, "Actively quenched single-photon avalanche diode for high repetition rate time-gated photon counting", *Review of Scientific Instruments*. 67 (1), January (1996).

[13].Li-Qiang Li and Lloyd M. Davis "Single photon avalanche diode for single molecule detection", *Review of Scientific Instruments*. 64 (6), June (1993).

[14].Samuel T. Hess and Watt W. Webb, "Focal Volume Optics and Experimental Artifacts in Confocal Fluorescence Correlation Spectroscopy", *Biophysical Journal* . 83, 2300 – 2317 October (2002).

[15].Shuming Nie, Daniel T. Chiu, and Richard N. zare, "Real-Time Detection of Single Molecules in Solution by Confocal Fluorescence Microscopy" *Analytical Chemistry*, 67,2849-2857(1995).

[16].Ming Zhao, Lei Jin, Bo Chen, Yao Ding, Hui Ma, and Dieyan Chen, "Afterpulsing and its correction in fluorescence correlation spectroscopy experiments" *Applied Optics,* 42, 19 July (2003).

[17].M. A. Medina and P. Schwille, "Fluorescence correlation spectroscopy for the detection and study of single molecules in biology," *BioEssays* 24,758-764 (2002).

Vita

You Li was born in the Chongqing, China. She received her undergraduate degree at Sichuan University in China, in June 2007. Since August 2007, she has been at UTSI working towards her Masters in Physics.